

Seasonal and decadal variation in phytoplankton absorption and non-algal particulate matter in the Northwest Atlantic

Emmanuel Devred¹, Tim Perry¹ and Philippe Massicotte^{2,*}

¹ Ocean and Ecosystem Sciences Division, Bedford Institute of Oceanography, Fisheries and Oceans Canada, Dartmouth, NS, Canada

¹ Département de Biologie, Tukuvik Joint International Laboratory/UMI 3376, ULAVAL (Canada) – CNRS (France), Université Laval, Québec, QC, Canada

Correspondence*:

Emmanuel Devred

emmanuel.devred@dfo-mpo.gc.ca

2 ABSTRACT

3

4 **Keywords:** Phytoplankton, absorption, chlorophyll-a concentration, phytoplankton apparent absorption wavelength (*PAAW*), Northwest
5 Atlantic, Time series analysis

1 INTRODUCTION

6 Underwater light characteristics are important drivers of ecological processes. Among others, the magnitude
7 of the primary productivity of photosynthetic communities (Platt and Gallegos, 1980) and the photodegra-
8 dation of organic matter (Moran and Zepp, 1997) are directly influenced by the quality and quantity of light
9 penetrating the water column. The optically active constituents (OACs) controlling water's inherent optical
10 properties (IOPs), such as light absorption and scattering, in one ecosystem may differ fundamentally
11 from those in another. In open water environments where the optical properties of the ocean are driven
12 by phytoplankton, commonly referred to as case 1 waters (Morel and Prieur, 1977), absorption by phyto-
13 plankton and its detrital matter plays a key role in regulating the underwater lightscape as phytoplankton
14 absorption alone represents more than 50% of the total light absorption budget (Oubelkheir et al., 2007;
15 Mascarenhas et al., 2017). An extensive literature has established empirical relationships between water
16 OACs (mostly chlorophyll-a concentration and associated pigments) and their IOPs in the open oceans (e.g.
17 Gordon and McCluney, 1975; Morel and Bricaud, 1981; Mobley, 1994; Bricaud et al., 1995; Cleveland,
18 1995; Bricaud et al., 1998; Ciotti et al., 2002; Bricaud et al., 2004; Devred et al., 2006; Bricaud et al.,
19 2010; Brewin et al., 2011), and coastal (Babin et al., 2003) and polar aquatic environments (Matsuoka
20 et al., 2014; Ferreira et al., 2017). The absorption coefficient of phytoplankton, a_ϕ (m^{-1}), has often been
21 used as a proxy for phytoplankton biomass. It is also known to be highly influenced by the growing
22 conditions and the physiological state of the algal assemblage and may not always truly represent the
23 carbon content of phytoplankton cells (Behrenfeld et al., 2006). Phytoplankton absorption magnitude and
24 spectral dependence also inform on phytoplankton community structure (Hirata et al., 2008) and have been
25 used in primary production models, either directly to retrieve production (Marra et al., 2007) or indirectly
26 to weight phytoplankton light harvesting efficiency (Morel, 1978; Kyewalyanga et al., 1997). Along with
27 a_ϕ , the chlorophyll-specific absorption coefficient (a_ϕ^* , absorption per unit concentration of chlorophyll-a in

28 $\text{m}^2 \text{ mg}^{-1}$) varies with changes in phytoplankton intracellular composition and concentration, and pigment
29 packaging effect (Duysens, 1956; Mitchell and Kiefer, 1988; Kirk, 1976; Bricaud et al., 1995, 2004). The
30 exploitation of these features has led to the determination of phytoplankton size classes and taxonomic
31 groups in natural water samples using optical satellites (Ciotti et al., 2002; Devred et al., 2006, 2011; Fujiki
32 and Tagushi, 2002; Sathyendranath et al., 2004; Brewin et al., 2011). Because phytoplankton absorption is
33 characterized by a wide peak around 443 nm and a sharp maximum around 675 nm, empirical relationships
34 usually focus on these two wavelengths rather than fully exploiting the spectral information contained
35 in absorption measurements (Babin et al., 2003; Bricaud et al., 1995; Aiken et al., 2007). Still, these
36 indices have been proven useful to study the phytoplankton dynamics in aquatic ecosystems. Absorption
37 by non-algal particles, a_{NAP} (m^{-1}), a “methodological by-product” of the determination of phytoplankton
38 absorption derived from total particulate absorption, a_p (m^{-1}), has been less studied than phytoplankton
39 absorption even if its role in shaping the underwater lightscape is not negligible. Its spectral resemblance to
40 the colored dissolved organic matter absorption spectrum has often resulted in lumping both absorptions
41 together when solving radiative transfer issues (Hoge and Lyon, 1999; Maritorena et al., 2002; Werdell
42 et al., 2018). Bricaud et al. (1998) found a significant relationship between chlorophyll-a concentration
43 and a_{NAP} , however the relationship between these two variables may be location-dependent (Sosik and
44 Mitchell, 1992). The ratio between a_p and a_{NAP} has been found to be as low as 10% at the surface in open
45 oceans and reach 20% to 30% at depth (Bricaud et al., 1998), while it can dominate the absorption budget
46 in coastal areas (Babin et al., 2003; Williams et al., 2018; Kratzer and Moore, 2018).

47 Long-time series of *insitu* measurements at high spatial resolution are difficult to acquire due to financial
48 and logistical constraints. Hence, samplings in ecological studies are often carried out at a single location
49 over a short period of time focusing on a single process such as the algal spring bloom event, or by
50 combining data from various field campaigns that were carried out in different locations and times (Bricaud
51 et al., 2004; Devred et al., 2006), which hinder our understanding of the seasonal dynamics of phytoplankton
52 absorption. In the current study, we used an extensive and comprehensive dataset acquired within the
53 Atlantic Zone Monitoring Program (AZMP Casault et al., 2020) and Atlantic Offshore Zone Monitoring
54 Program (AZOMP Yashayaev et al., 2021) frameworks made of water samples collected over the last 20
55 years to describe in details the seasonal variability of chlorophyll-a concentration ($[\text{Chl-a}] \text{ mg m}^{-3}$), a_ϕ and
56 a_{NAP} as well as their relationships in three regions of the Northwest Atlantic. We also used information on
57 fucoxanthin concentration ($[\text{Fucox}] \text{ mg m}^{-3}$) as an indicator of diatom presence to help interpret the results.
58 We also address the challenge of using hyperspectral information, namely phytoplankton absorption, in
59 environmental studies to determine the status of the marine ecosystem given its complex interpretation due
60 to its wide variation over the visible spectrum, such that the use of one or two wavelengths only truncates
61 the information contained in an entire spectrum. We present a simple absorption index for phytoplankton
62 absorption (i.e., Phytoplankton Apparent Absorption Wavelength, $PAAW$) that was inspired by the work of
63 Vandermeulen et al. (2020) who applied this concept to remote sensing reflectance. This index summarizes
64 all the spectral information contained in a given phytoplankton absorption spectra into a single number
65 (nm) that provides information on the biomass and structure of the phytoplankton community by passing
66 the need for chlorophyll-a concentration measurements. Our large datasets provided the ability to detect
67 possible changes in $PAAW$ at the regional scales over two decades and to test the minimum sampling
68 requirement to capture the natural variability of the Northwest Atlantic ecosystem.

2 MATERIAL AND METHODS

69 2.1 Study area and sampling

70 Since 1999, the Department of Fisheries and Oceans Canada (DFO) conducts annual surveys in the
71 Northwest Atlantic as part of the Atlantic Zone and Atlantic Offshore Zone monitoring programs Therriault
72 et al. (1998); Pepin et al. (2005). Each year, in spring sometimes between April and June, depending on
73 ship availability and weather, about 100 stations are sampled on the Scotian Shelf/Gulf of Maine region and
74 28 stations are sampled in the Labrador Sea along a transect that spans from the Labrador Shelf (Canada) to
75 the Greenland Shelf (Denmark), crossing the Labrador Basin (Figure 1). The spring cruise on the Scotian
76 Shelf is repeated in the fall from mid-October to mid-November. Fish surveys that happened during winter
77 and summer opportunistically provided additional water samples. For this study, a total of 3279 sampling
78 events were compiled and grouped into three bioregions, namely the Scotian Shelf, a temperate mesotrophic
79 environment, the Northwest Atlantic Basin, and a temperate oligotrophic environment and the Labrador
80 Sea, a sub-arctic environment. The delineation of these bioregions was based on bathymetry (GEBCO2021)
81 and the latitude (Supplementary Figure S1): (1) Scotian Shelf (bathymetry < 600 m and latitude < 48°N),
82 (2) Northwest Atlantic Basin (bathymetry ≥ 600 m and latitude < 48°N) and (3) Labrador Sea (latitude
83 ≥ 48°N). Observations were further grouped into seasons based on the time of sampling (Supplementary
84 Figure S1B): spring (Mar, Apr, May, N = 1598), summer (Jun, Jul, Aug, N = 369), autumn (Sept, Oct,
85 Nov, N = 1174) and winter (Dec, Jan, Feb, N = 138). At each station, surface water (< 30 m) was collected
86 to measure phytoplankton pigment composition and particulate absorption.

87 2.2 Data and laboratory analysis

88 2.2.1 Chlorophyll-a and Fucoxanthin pigment concentration

89 Samples for pigment analysis were filtered at low pressure (< 10 dpi) on 25 mm WF/F Whatman filters
90 (sterlitech Grade F Glass microfiber) with 0.2 μm mesh size and immediately flash frozen and stored in
91 Nitrogen Liquid during the sea-going fieldwork. The volume of filtration varied between 0.25 and 1 L
92 based on a visual inspection of the filter colour to ensure that enough material was retained for analysis.
93 Upon return to the Bedford Institute of Oceanography, the samples were stored inside a -80° C freezer until
94 analysis in the laboratory. Pigments composition and concentration were measured on a Beckman–Coulter
95 Gold High-Performance Liquid Chromatography (HPLC) system between 1998 and 2013, and on an
96 Agilent 12000 HPLC system for data collected between 2013 and 2020. Details on the HPLC method
97 to extract and measure pigment concentration can be found in Head and Horne (1993). In this study, we
98 limited the pigment to chlorophyll-a and derivative ([Chl-a] in mg m^{-3}) and fucoxanthin ([Fucox] in mg
99 m^{-3}) concentration, the latter being used as a coarse indicator of diatom presence in samples.

100 2.2.2 Absorption coefficient of phytoplankton and non-algal particulate matter

101 Filtration for phytoplankton (a_ϕ) and non-algal particles (a_{NAP}) absorption coefficients were carried out
102 simultaneously as filtration for pigment analysis following the same protocol (i.e., filtration and storage
103 method). Phytoplankton absorption coefficients between 350 and 750 nm were measured at 1 nm increment
104 on a UV-Vis Shimadzu 2600i double beam with an integrating sphere in transmission mode. Only the
105 visible part of the spectrum (400-700 nm) was used in the current study. Total particulate absorption
106 coefficient (a_p) was measured first, after which, the filter was soaked in hot methanol for 25 to 45 minutes
107 to extract phytoplankton pigments. The absorption by non-algal particles, also referred to as detritus
108 absorption, was then measured, and phytoplankton absorption was inferred by subtraction of a_{NAP} to a_p as
109 described in Mitchell and Kiefer (1984) following modifications by Hoepffner and Sathyendranath (1991)
110 and Kyewalyanga et al. (1997). The pathlength correction (i.e., the β -factor) was computed as in Stramski
111 et al. (2015). Two quality control procedures were used to ensure the integrity of the absorption dataset;

112 spectra were removed from further analysis if: (1) negative values occurred between 350 and 400 nm and
 113 (2) the absorption coefficient at 410 nm was higher than the one at 443 nm as in Devred et al. (2006). The
 114 slope of the exponential decrease of the particulate absorption spectrum, S_{NAP} was computed by fitting
 115 the following equation to the data using the *nls()* function in R over the range 400 to 700 nm excluding
 116 the 400 to 480 and 620 to 700 nm ranges to avoid possible contamination by pigment remaining from the
 117 extraction:

$$a_{NAP}(\lambda) = a_{NAP}(443)(-S_{NAP}(\lambda - 443)). \quad (1)$$

118 2.3 Statistical Analysis

119 2.3.1 Phytoplankton apparent absorption wavelength

120 To summarize the spectral information contained in phytoplankton absorption measurements in a simple
 121 index, we used a method similar to that of Vandermeulen et al. (2020). The formulation of this index
 122 was initially proposed to maximize the utilization of the spectral information contained in remote sensing
 123 reflectance, and simply represents the weighted harmonic mean of a spectrum. As pointed out by Van-
 124 dermeulen et al. (2020), but adapted to our study (what was adapted exactly?), the index indicates the
 125 wavelength balance point around which absorption is evenly distributed. Since we are adopting this index to
 126 characterize the spectral shape of in situ phytoplankton absorption, we named this index the phytoplankton
 127 apparent absorption wavelength (*PAAW*, nm), which was calculated as follows:

$$PAAW = \frac{\sum_{\lambda=400}^{\lambda=700} a_\phi(\lambda)}{\sum_{\lambda=400}^{\lambda=700} a_\phi(\lambda)/\lambda} \quad (2)$$

128 Where $a_\phi(\lambda)$ is the measured phytoplankton absorption measured at the wavelength λ (nm).

129 2.3.2 Regression and trend analysis

130 The relationship between phytoplankton absorption coefficient at a given wavelength and [Chl-a] was
 131 derived using a type-2 linear regression on the log10-transformed data (when required to achieve normality).
 132 Times series analysis of the *PAAW* was performed on data collected in spring and autumn only (except
 133 for the Labrador Sea in autumn), as there were no sufficient years with data in winter and summer to obtain
 134 reliable trends. For all-time series, namely the entire dataset, the three datasets partitioned into regions
 135 and the five datasets partitioned into seasons and regions, the mean *PAAW* was computed and its trend
 136 was derived using a weighted general linearized model (*glm()* in R). The weights for the fit were derived
 137 using the number of data available in any given year/region/season and the model included the latitude
 138 and longitude to account for any possible geographical bias in the linear regression due to sampling. The
 139 coefficient derived for the annual independent variable was used to describe the trend.

140 All data manipulation and statistical analysis were performed in R 4.1.2 (refs) and all the data used in
 141 this study are available on Zenodo (add link). The R packages used in the study include: [include list here](#)

142 All these extra analyses with lon lat, glm etc. that were requested, are not used?

3 RESULTS

3.1 [Chl-a], [Fucox], absorption coefficients and PAAW seasonal and regional variations

For the three biogeochemical regions, both mean [Chl-a] and [Fucox] were highest in spring when phytoplankton bloom and the community assemblage is dominated by diatoms with values of 2.70, 1.80 and 2.73 mg m⁻³ for [Chl-a] on the Scotian Shelf, NAB and the Labrador Sea, respectively, and values of 0.89, 0.47 and 0.72 mg m⁻³ for [Fucox] on the Scotian Shelf, NAB and the Labrador Sea, respectively (Table 1). The Scotian Shelf showed the highest seasonal variability with a strong decrease of both [Chl-a] and [Fucox] in summer followed by an increase during fall and a second decrease in winter for [Chl-a] that remained higher than the mean summer values, while [Fucox] in winter was greater than in Fall (Figure 2). Both [Chl-a] and [Fucox] in NAB followed the same seasonal pattern as on the Scotian Shelf, but with smaller mean values. The Labrador Sea exhibited a different seasonal cycles than the two other regions, as both [Chl-a] and [Fucox] continuously decreased during summer, fall and winter to reach the lowest values of all regions and seasons (i.e., [Chl-a] = 0.19 mg m⁻³ and [Fucox] = 0.05 mg m⁻³). The similar seasonal cycle between [Chl-a] and [Fucox] is supported by the high degree of correlation between the two pigments (0.85, Figure 3)

Measured absorption coefficients at 443 nm for particulate, non-algal and phytoplankton spanned about three orders of magnitude and followed a normal distribution when log₁₀-transformed (Figure ??). All properties showed large regional and seasonal variabilities (Table 1 and figure 3, fig3 is showing only 2 parameters). Data revealed the same seasonal cycle for $a_\phi(443)$ than for [Chl-a] with the exception that $a_\phi(443)$ was slightly higher in the fall (0.059 m⁻¹) than in the spring (0.050 m⁻¹) on the Scotian Shelf (Fig. xxx). The absorption coefficient at 675 nm (Fig. 2B, we have so (too) many figures in the paper, have to hold the hand of the reader and point out every figure/panel to support the text) exhibited the same seasonal cycle as $a_\phi(443)$ with smaller values as expected. The specific absorption coefficient at 443 nm showed an inversed pattern to [Chl-a] and $a_\phi(443)$ in all regions, perhaps with less variability between summer and fall on the Scotian Shelf compare to $a_\phi(443)$ and the notable exception of the low mean $a_\phi^*(443)$ in the Labrador Sea when [Chl-a] is also low. Absorptions coefficient at 443 nm by non-algal particulate matter exhibited a different seasonal pattern than $a_\phi(443)$ on the Scotian Shelf, with high values reached in the spring followed by a decrease in Summer and an increase for both fall and winter. In the NAB, $a_{NAP}(443)$ was highest in spring, with values relatively low (0.0051 m⁻¹) compared to the Scotian Shelf (0.009 m⁻¹) and Labrador Sea (0.0075 m⁻¹). For the rest of the year, $a_{NAP}(443)$ remained quasi constant with values of about 0.0035 m⁻¹ (ANOVA test p-value > 0.05). In the Labrador Sea, $a_{NAP}(443)$ showed a similar seasonal pattern to $a_\phi(443)$ with a continuous decrease from spring to winter, unlike the two other regions where markedly different seasonal patterns were observed. The slope of the NAP absorption spectrum also shows very weak seasonal dependence, with a slight decrease from spring to winter on both the Scotian Shelf and NAB, while S_{NAP} reaches a minimum in fall in the Labrador Sea.

The PAAW provided additional information than [Chl-a], $a_\phi(443)$ and $a_\phi^*(443)$. On the Scotian Shelf, PAAW exhibited a seasonal cycle that resembled the one of $a_\phi^*(443)$ with a mean value of 483 nm in Spring that decreased to 470 nm in Summer to increase again in autumn (478 nm) and winter (481 nm). In the NAB, PAAW followed a similar pattern to $a_\phi(443)$ and $a_\phi(675)$; PAAW in all seasons being smaller than the PAWW observed on the Scotian Shelf. Interestingly, the PAAW in the Labrador Sea showed a different pattern than the $a_\phi^*(443)$ and $a_\phi(443)$ ones, associated with the lower seasonal variability (461-498). The PAAW was higher in Spring and Fall (maybe use autumn, like in the figures, verify everywhere) than in Summer and Winter (summer and autumn are pretty similar).

186 **3.2 Bio-optical relationships: [Chl-a], $a_\phi(443)$, $a_{NAP}(443)$ and S_{NAP}**

187 You are about to talk about figure 4 but have not presented fig3. Should be presented in order of
 188 appearance.

189 The [Chl-a]: $a_\phi(\lambda)$ is arguably the most studied of all the bio-optical properties. When grouping all the
 190 data together, independently of regions and seasons, the linear regression of $a_\phi(443)$ against [Chl-a] in the
 191 log₁₀ space can be described in the linear space as:

$$a_\phi(443) = 0.0407[\text{Chl-a}]^{0.515}, \quad (3)$$

192

193 The coefficient of the power-law fit provided a factor close to the one found by Bricaud et al. (1998)
 194 (Figure 4A) who reported a value of 0.0378, but with a smaller exponent (i.e., 0.627 in Bricaud et al.
 195 (1998)). Bricaud et al. (2004) derived coefficients for the [Chl-a]: $a_\phi(443)$ relationship that was larger than
 196 the one found here with values of 0.0654 and 0.728 (where these 2 numbers come from?, I do not see them
 197 in Fig. 4) for the factor and exponent respectively. The correlation coefficient in the current study is much
 198 smaller than the ones found by Bricaud et al. (1998) and Bricaud et al. (2004), which were equal to 0.90
 199 and 0.93 respectively, however, they computed their correlation coefficient on a linear scale, while we
 200 provided the R^2 here for the log₁₀-transformed data (I do not understand the "however". It is "not" good for
 201 us if we have a lower R2 and using log-log regressions...). The relationship found here remained consistent
 202 with the one found by Devred et al. (2006), which was established using some of the data included in the
 203 current study. In general, all models agreed well in the bulk range of [Chl-a] between 0.3 and 5 mg m⁻³ and
 204 discrepancies between models occurred mainly in the extreme range of values. The regional relationships
 205 exhibited a large difference in the exponent with values of 0.469, 0.508 and 0.616 for the Scotian Shelf,
 206 NAB and the Labrador Sea respectively, while the intercept in the linear space remained similar and varied
 207 between 0.038 and 0.042 (where do you see all these values?) for the three regions (Figure 4C-D). The
 208 Scotian Shelf showed the lowest R^2 , with a value of 0.53 that may be driven by seasonal variations. As for
 209 the [Chl-a]- $a_\phi(443)$ relationship, the $a_{NAP}(443)$: $a_\phi(443)$ showed regional differences in all three regions,
 210 but with $a_\phi(443)$ dominating the particulate absorption (Figure 4). High variability around the model was
 211 consistent with low correlation coefficients, in particular on the Scotian Shelf. The slope of the linear
 212 regression of $a_{NAP}(443)$ against $a_\phi(443)$ was 0.108 ($R^2=0.32$), 0.063 ($R^2=0.23$) and 0.070 ($R^2=0.31$)
 213 for the Scotian Shelf, Northwest Atlantic Basin and Labrador Sea respectively (I do not see these numbers
 214 on the figure).

215 It has been shown that the sum of diagnostic pigments (i.e., pigments that are used as taxonomic group
 216 markers such as peridinin, fucoxanthin, zeaxanthin and chlorophyll-b) are highly correlated with [Chl-a]
 217 (Claustre, 1994; Vidussi et al., 2001; Uitz et al., 2006; ?). [Fucox] was strongly correlated to [Chl-a] with a
 218 slope of X ($R^2 = Y$) in agreement with previous work (Claustre, 1994)

219 **3.3 Spectral variation in phytoplankton absorption**

220 A simple method to analyse the spectral variation of phytoplankton absorption relies on the study of
 221 $a_\phi(443)$: $a_\phi(675)$ ratio as a function of [chlorophyll-a concentration], which provides a rapid assessment
 222 of the packaging effect and therefore a rough estimation of community structure (Bricaud et al., 2004;
 223 Devred et al., 2006; Vishnu et al., 2018). At the Northwest Atlantic scale, both [Chl-a] and [Fucox] were
 224 both correlated highly correlated to $a_\phi(443)$: $a_\phi(675)$ with R^2 of 0.72 and 0.76 respectively (which Fig?).
 225 The slope of the regression of log₁₀-transformed $a_\phi(443)$: $a_\phi(675)$ against [Chl-a] was 0.21. The slope of
 226 the regression was lower in the Labrador Sea (i.e., 0.165) compared to the other two bioregions (0.219)

and 0.231 for the Scotian Shelf and Northwest Atlantic Basin respectively, Figure ??). [Chlorophyll-a] was slightly more correlated with $a_\phi(675)$ ($R^2 = 0.89$) compared to $a_\phi(443)$ ($R^2 = 0.81$) hinting that other pigments might contribute to absorption in the blue part of the absorption spectrum.

Another way of summarising spectral variation in phytoplankton absorption is to use the *PAAW* (see section 2.3.1), which accounts for contribution from all wavelengths rather than only two (i.e., 443 and 675 nm). The *PAAW* showed that the spectral shape of the phytoplankton absorption varied across the three bio-regions (Figure 7). For the three regions, a large *PAAW* corresponds to normalized spectra with the flattest shape, where the difference between the blue and red absorption peak is the smallest (Figure 7A). As the *PAAW* decreases, phytoplankton in the blue part of the spectrum increases and a shoulder occurs around 490 nm. The Scotian Shelf showed the highest variability in *PAAW* with some of the “bluest” waters with *PAAW* as high as 500 nm (Figure 7B). The distribution of *PAAW* on the Scotian Shelf shows a bimodal shape with a second small bump located in the blue part of the *PAAW* (I do not see a bump in the blue). The Labrador Sea region exhibited the narrowest range of variation for the *PAAW* index, with a mean value similar to the Scotian Shelf. Similar to the Scotian Shelf, the distribution exhibited a bimodal mode with a second small peak in the blue range. Finally, the NAB region has a quasi-normal distribution (I would not use this here, they all look “normal”) of the *PAAW*, which is centred on 476 nm, which corresponds to the smallest *PAAW* of the three regions. The mean *PAAW* shows that phytoplankton absorption spectra were slightly more shifted in the blue part of the spectrum in the Scotian Shelf and the Labrador Sea compared to the spectra measured in the Northwest Atlantic Basin. *PAAW* was positively correlated to [Chl-a] and negatively ($a_\phi^*(443)$) (Figure 8A and B). A second-order polynomial equation was used to model the decrease of the $a_\phi(443):a_\phi(675)$ ratio with increasing *PAAW* (Figure 8C). Higher values of *PAAW* were associated with low values of the ratio in the spring. A higher spread in the data occurred at lower *PAAW* (Figure 8C). The variance in [Chl-a] was slightly better explained by *PAAW* ($R^2 = 0.69$) than by $a_\phi(443)$ (Figure 4, $R^2 = 0.65$). Using *PAAW* to predict the $a_\phi(443):a_\phi(675)$ ratio compared to [Chl-a] increased R^2 from 0.72 to 0.87 (Figure 8C).

Slopes about what? 8A-B and C?

Trend analysis of the *PAAW* for the entire dataset and all regions did not show any significant changes, all the trends were positive but with a p-value that remained high (why are you not using weight-averaged results as requested?). However, trend analysis at the regional and seasonal level revealed a significant increase in the *PAAW* in all three regions in spring (Table 2 and Figure 9). The Scotian Shelf exhibited the highest rate of change with a slope of 0.38 nm y^{-1} followed by the Labrador Sea (0.25 nm y^{-1}) and the NAB (0.18 nm y^{-1}). The fall showed an opposite trend a decrease in the *PAAW* on both the Scotian Shelf (-0.15 nm y^{-1}) and the NAB (-0.31 nm y^{-1}), while there were no sufficient years to compute reliable statistics in the Labrador Sea in Autumn and all regions in Summer and Winter.

You are not talking about your Fig. 10. A lot of appendix figures are not discussed.

4 DISCUSSION

In the current study, we have used an extensive dataset of several bio-optical parameters, measured in space and time, to examine their variability and linkage. In general, our results agreed, and reinforced, current knowledge about phytoplankton biomass and community structure, depicted using [Fucox] as a very rough indicator of diatom presence, and their relationships to phytoplankton and non-algal particulate absorptions. The added value of our current study relies upon the quantification of the spatio-temporal variations in bio-optical properties and their trends at decadal scales. While most studies relies on a single cruise (Stuart et al., 2000; Pérez et al., 2021), a combination of cruises gathered from one region (Ferreira

et al., 2013; Matsuoka et al., 2014) or the global ocean without a pre-defined temporal strategy (Trees et al., 2000; Ciotti et al., 2002; Bricaud et al., 2004; Brewin et al., 2011), the DFO monitoring cruises have systematically carried out measurements of bio-optical properties at about 150 stations spanning about 20° in latitudes (i.e., 42 to 62°N) in covering the entire seasonal cycle for more than 20 years resulting in a unique dataset that provided robust knowledge on the Northwest Atlantic (NWA) Ecosystem (this was already said in the abstract, introduction and methods). The NWA was divided into three regions with markedly different regimes what kind of regime?: 1) The Scotian Shelf showed a regime of a mid-latitude shelf environment, with high seasonal variations in biomass and associated properties, 2) the NAB showed the dynamic of an oligotrophic environment, with low biomass compare to the two other regions and a more subtle seasonal cycles and finally 3) the Labrador Sea exhibited the characteristics of a sub-arctic environment with a delayed spring growth in phytoplankton biomass what makes you assess it is delayed? Cite figure or results, that remained sustained over the Summer to slowly decrease in Autumn and reach low levels in Winter when light and sea ice are limiting factors to phytoplankton production. The impacts of these various regimes on the bio-optical properties of the NWA are discussed in the following sections.

4.1 Phytoplankton biomass and absorption in the Northwest Atlantic

The coefficients of the power-law that expressed $a_\phi(443)$ as a function of [Chl-a] (Eq. 3.2) were consistent with previous studies, the main differences occurred in the extreme ranges of the relationship and can be attributed to the range of variations of the bio-optical properties and the type of water sampled in previous studies. For instance, the higher coefficients found by Bricaud et al. (2004) compared to the current study can be explained by the oligotrophic waters that were sampled in their study. This is also highlighted in the regional differences that we found between the three regions of the Northwest Atlantic as emphasized by Stuart et al. (2000) who showed that diatom-dominated waters of the Labrador Sea exhibited a lower absorption coefficient per unit of [chlorophyll-a concentration] than water dominated by prymnesiophytes. This led to the development of satellite-based algorithms to identify diatoms occurrence (Sathyendranath et al., 2004) in the Northwest Atlantic. Seasonal changes in light irradiance reaching the water surface, temperature and nutrient availability are among the main drivers that regulate the size structure, the intracellular pigment composition and the absorption characteristics of the algal populations (Ciotti et al., 2002; Bricaud et al., 2004; Churilova et al., 2017). The spring bloom in the NWA is dominated by diatoms in all three regions which result here suggests that diatoms dominate over other groups?, in agreement with phytoplankton enumeration carried out at a fixed station on the Scotian Shelf (Casault et al., 2020), which is consistent with the low specific absorption and high [Fucox] observed during that time (Table 1). The fall bloom on the Scotian Shelf and in the NAB exhibited $a_\phi^*(443)$ that were much higher than during the spring, despite relatively high phytoplankton biomass, suggesting that large phytoplankton than diatoms (e.g., dinoflagellates) dominated the phytoplankton assemblage and were associated with low packaging effect (please cite the corresponding figure). Species succession in the Labrador Sea we do not have data that show a species succession even if in the reality it is likely there are, based on the optical traits, showed a different pattern with a continuous decrease (increase) of phytoplankton biomass ($a_\phi^*(443)$). While high biomass and dominance of diatoms have been established in spring in the Labrador Sea using both phytoplankton counts and pigment composition (Fragoso et al., 2017, 2018), the present study reveal for the first time the entire annual cycle of phytoplankton assemblage with large cells that dominated the spring and summer signal while small cells dominate the optical signal during the autumn and winter. Although no direct measurements of the phytoplankton cell size were made during the DFO oceanographic cruises, rich literature has proven that inferences could be made from the measured IOPs. For instance, results from Fujiki and Tagushi (2002) indicated that a decrease in $a_\phi(675)$ was solely associated with increasing phytoplankton cell volume and packaging effect. Likewise, Bricaud et al. (1995) found

that increase in [Chl-a] was negatively correlated with both $a_\phi^*(443)$ and the blue-to-red phytoplankton absorption ratio (see Figure 8) that was further attributed to an increasing pigment packaging and lower proportion of accessory pigments (Staehr et al., 2004; Vishnu et al., 2018). Here we found a decrease of the $a_\phi^*(443) : a_\phi^*(675)$ with [Fucox] for the entire dataset with a slope of -0.163, which is consistent with the results of Hoepffner and Sathyendranath (1993) who found an increase of $a_\phi(440) : a_\phi(550)$ with [Fucox] from 0.05 to 0.3 depending on the phytoplankton assemblage. While Hoepffner and Sathyendranath (1993) used a different phytoplankton absorption ratio, the results point in the same direction of the change in phytoplankton spectral shape with changes in phytoplankton community structure.

Spatio-temporal variations of non-algal particulate absorption magnitude and spectral dependence showed complex patterns (fig xx). The dataset encompassed a wide range of variations in both $a_{NAP}(443)$ and S_{NAP} certainly due to the type of water sampled, which included mesotrophic coastal environments on the Scotian Shelf, oligotrophic waters of the NAB and sub-arctic waters of the Labrador Sea. However, several patterns emerged at the regional scale, $a_{NAP}(443)$ remained below 11% of $a_\phi(443)$ in general, with the highest percentage observed in the mesotrophic environment of the Scotian Shelf and the lower values occurring in the NAB (fig. xxx). Large discrepancies were observed around the mean relationship (Figure 5) suggesting that many short-term processes may be included in the production of detritus from living phytoplankton (i.e., grazing, viral lysis) that were captured by the repeated sampling. However, only a study at high temporal frequency sampling (i.e., several times a day for several days) may reveal the processes included in the degradation of phytoplankton and lead to a detailed understanding of the absorption dynamics of phytoplankton and non-algal particles. Diatom-dominated phytoplankton biomass we have the data to prove/show that?, indicated by [fucox] was associated with high $a_{NAP}(443)$ and high S_{NAP} . For instance, relatively high [Chl-a] and [Fucox] on the Scotian Shelf (2.7 and 0.89 mg m⁻³, respectively) and Labrador Sea in Spring (2.7 and 0.72 mg g⁻³, respectively) were associated with high $a_{NAP}(443)$ (0.009 and 0.0075 m⁻¹ for the Scotian Shelf and Labrador Sea, respectively) and S_{NAP} (0.0124 and 0.0134 m⁻¹ for the Scotian Shelf and Labrador Sea, respectively). On the other hand, low [Chl-a] and [Fucox] in the NAB in summer were associated with low $a_{NAP}(443)$ and S_{NAP} . A departure from this pattern was the high [Chl-a] and low [Fucox] associated with relatively low $a_{NAP}(443)$ and S_{NAP} on the Scotian Shelf in Autumn. Magnitude and spectral absorption by detritus may depends on the phytoplankton assemblage and its degradation through biogeochemical processes (e.g., virus infection, Nagasaki, 2008). The spring bloom also corresponds to the maximum of zooplankton abundance on the Scotian Shelf (Casault et al., 2020) and a number of studies have demonstrated the selective feeding of zooplankton towards diatoms (Teegarden et al., 2001; Leising et al., 2005). Grazing by zooplankton produces phaeopigments (Shuman and Lorenzen, 1975; Head and Horne, 1993; Collos et al., 2005) and increases the concentration of detritus (i.e., non-algal particles) in the water column and therefore its absorption. These processes suggest that the spectral slope of the absorption by NAP might be impacted by community structure and zooplankton grazing, however, this statement would need to be further studied. Our results, however, support that zooplankton grazing may have an impact on the bulk optical properties of seawater and the emergence of new sensors with hyperspectral capability may help inform secondary production using variation in a_{NAP} as an indicator of zooplankton grazing activity.

4.2 The phytoplankton apparent absorption wavelength (PAAW): an integrative index of the spectral shape of phytoplankton absorption

Retrieval of pigments concentration from absorption spectrum has been carried out in the past using gaussian decomposition (Hoepffner and Sathyendranath, 1991; Chase et al., 2013; Zhang et al., 2021), machine learning (Chazottes et al., 2006; Bricaud et al., 2007) and derivative analysis (Bidigare et al., 1989; Catlett and Siegel, 2018) to cite a few methods. Here we used an integrative index and related it to

phytoplankton bio-optical properties. The takeaway message from this index is that it performed slightly better, in terms of R^2 , than any other variable, namely $a_{\text{Chl-a}}$, $[{\text{Fucox}}]$, $a_{\phi}(443)$ and $a_{\phi}^*(443) : a_{\phi}^*(675)$ when studying the triangular relationship between absorption, biomass and community structure. The *PAAW* provided information on the trophic status as supported by the high correlation coefficient with $[{\text{Chl-a}}]$, which was slightly greater than the $[{\text{Chl-a}}] - a_{\phi}(443)$ one (i.e., 0.65). The other advantage of the *PAAW* that it can also be used to describe the community structure given its high correlation to $a_{\phi}(443) : a_{\phi}(675)$ ($R^2 = 0.88$) and $[{\text{Fucox}}]$ ($R^2 = 0.6941$). Analysis of the phytoplankton absorption spectral variation showed consistency with *PAAW* and notably, non-linear changes in the absorption spectra from small-cell to large-cell that translated into a decrease in *PAAW* (which fig?). Another advantage of the *PAAW* is that its variation on a linear scale, compare to other bio-optical parameters that are expressed in \log_{10} , makes it a valuable index to report on changes in the environment and support decision making. For instance, the *PAAW* could be used for long-term monitoring, as shown by our time series analysis. Seasonal and regional analysis of *PAAW* revealed a shift in phytoplankton biomass in Spring towards smaller *PAAW* (e.g., blue) suggesting a decrease in the packaging effect and abundance of large phytoplankton such as diatoms. This is consistent with a recent satellite-based study that reveals an overall decrease in large phytoplankton in the biogeochemical provinces of the Northwest Atlantic (Liu et al., 2018). An opposite trend was observed in the autumn on the Scotian Shelf and NAB with a shift of *PAAW* toward the green wavelength, the shift was particularly important in the NAB. The *PAAW* might be a better indicator than $[{\text{Chl-a}}]$ to study the impact of climate change on phytoplankton biomass and community structure as (Dutkiewicz et al., 2019) demonstrated that changes in watercolour, as indicated by remote sensing reflectances, is a better indicator of changes in phytoplankton regimes as it includes information on changes in community structure. The *PAAW*, an index that accounts for both phytoplankton biomass and community structure, is easily understandable by a non-expert and provides valuable information on the phytoplankton regime in the marine ecosystem.

4.3 How many measurements do we need to characterize the bio-optical dynamics of an ecosystem?

out of scope of the paper

Sampling the ocean to study a given phenomenon (e.g., phytoplankton spring bloom) can be challenging given logistic constraints (ship availability and crew rotation) and the inherent temporal variation of ocean processes. Long-term monitoring programs with dates set in advance mitigate challenges as the repetitive measurements in space and time ensure that most oceanographic conditions will be encountered over years of field measurements. In the case of the spring bloom on the Scotian Shelf, given its variability in time (initiation varies over several weeks) and patchiness, the AZMP spring missions have sampled in many instances ante-, per- and post-bloom conditions as indicated by the wide range of $[{\text{Chl-a}}]$ measured (0.1 to 13 mg m^{-2}). The-optical relationships found in our study were in agreement with previous models (see section ??) emphasizing the universality of such relationships while supporting also the need to account for regional characteristics for fine-tuning. Our results explains the good performance of global algorithms such as the Ocean Land Colour Imager (OLCI) Neural Network $[{\text{Chl-a}}]$ algorithm (Hieronymi et al., 2017) or the QAA algorithm (Lee et al., 2002), which development relied on radiative transfer simulation that included the absorption models of Bricaud et al. (1995, 1998, 2004).

Long-term monitoring programs are needed to characterize trends and shifts in ecosystems, however, one can wonder to what effort sampling is needed to characterize the variability within an ecosystem. We addressed this question here by plotting the cumulative mean and standard deviation (SD) as a function of time for $[{\text{Chla}}]$, $a_{\phi}(443)$, $a_{NAP}(443)$ and S_{NAP} (Figure 10), assuming that when SD reaches an

403 asymptotic value, the variability of the ecosystem has been described. Our results suggest that about 5
404 years of sampling in Spring and Autumn on the Scotian Shelf were sufficient to capture the variability
405 in $a_{NAP}(443)$, while about 10 years were necessary for the Autumn. Standard deviations in [Chl-a] and
406 $a_\phi(443)$ reached their asymptotic values after 10 years. After 20 years of data collection, [Chl-a] and
407 $a_\phi(443)$ standard deviations have not converged yet in both Summer and Fall suggesting that the Scotian
408 Shelf is still undergoing significant changes during these two seasons and continuous sampling is required
409 to fully characterize the bio-optical dynamics of the Scotian Shelf.

5 CONCLUSION

410 Our study based on an extensive dataset collected at different times of the year in several oceanographic
411 regimes contributes to the knowledge of bio-optical properties of the Northwest Atlantic and in particular
412 the relationships between phytoplankton biomass and community structure on one side as indexed by
413 [Chl-a] and [Fucox] and absorption by phytoplankton and non-algal particles. Our dataset is made of
414 20-years of data collected over the four seasons of temperate latitudes describing in detail the seasonal
415 variation of bio-optical properties on the Scotian Shelf, Northwest Atlantic Basin and Scotian Shelf. This
416 paragraph is a repetition of what was said before a couple of times.

417 Using both traditional phytoplankton-based proxies and the *PAAW* index, results show that the cha-
418 racteristics of the phytoplankton and non-algal absorption in the Northwest Atlantic have undergone
419 significant changes over the past 20 years. The adopted *PAAW* index was found to provide equal or better
420 indications of the phytoplankton community compared with metrics that are traditionally measured during
421 oceanographic expeditions. An important aspect in favour of adopting the *PAAW* index is that it is solely
422 based on phytoplankton absorption spectra that are becoming routinely measured in situ by autonomous
423 platforms and profilers. Although additional controlled experiments are needed to evaluate the full potential
424 of *PAAW* to provide insights into phytoplankton community structure, the results of this study suggest
425 that it could be utilized as an efficient integrative index to obtain information on the underwater lightscape
426 characteristics in aquatic ecosystems.

CONFLICT OF INTEREST STATEMENT

427 The authors declare that the research was conducted in the absence of any commercial or financial
428 relationships that could be construed as a potential conflict of interest.

AUTHOR CONTRIBUTIONS

429 E.D. designed the study and assembled the dataset. E.D. and P.M. contributed to data analysis and
430 interpretation. P.M. computed all the statistics and made all the figures and drafted the manuscript. P.M.
431 and E.D. iterated the manuscript.

FUNDING

432 This study was supported by the Atlantic Zone Monitoring Program and Atlantic Zone Offshelf Monitoring
433 Program of the department of Fisheries and Oceans, Canada, in particular, the fieldwork and data analysis
434 in the laboratory. This study was made possible thanks to financial support from the Marine Environmental
435 Observation, Prediction and Response Network (MEOPAR). For further information about MEOPAR, visit
436 www.meopar.ca. This research was supported by the Sentinel North program of Universite Laval through
437 salary support for P. Massicotte, made possible, in part, thanks to funding from the Canada First Research
438 Excellence Fund.

ACKNOWLEDGMENTS

439 We are very grateful to the numerous Chief Scientists, scientists and Captain and crews of the Canadian
440 Coast Guard Ship who have relentlessly relayed over more than 20 years to build this unique dataset of
441 oceanographic properties. We particularly thank the captain and crew of the CCGS Hudson, as this research
442 vessel was used to collect the vast majority of the data presented in the study. The CCGS Hudson was
443 decommissioned this year. We also thank to the chairs of the AZMP and AZOMP programs who have
444 supported this research.

SUPPLEMENTAL DATA

445 Supplementary Material should be uploaded separately on submission, if there are Supplementary Figures,
446 please include the caption in the same file as the figure. LaTeX Supplementary Material templates can be
447 found in the Frontiers LaTeX folder.

DATA AVAILABILITY STATEMENT

448 The datasets [GENERATED/ANALYZED] for this study can be found in the [NAME OF REPOSITORY]
449 [LINK].

REFERENCES

- 450 Aiken, J., Hardman-Mountford, N. J., Barlow, R., Fishwick, J. R., Hirata, T., and Smith, T. J. (2007).
451 Functional links between bio-energetics and bio-optical traits of phytoplankton taxonomic groups: an
452 overarching hypothesis with applications for ocean-colour remote sensing. *J. Plankton Res.* 30, 165–181.
453 doi:10.1093/plankt/fbm098
- 454 Babin, M., Morel, M., Fournier-Sicre, V., Fell, F., and Stramski, D. (2003). Light scattering properties
455 of marine particles in coastal and open ocean waters as related to the particle mass concentration.
456 *Limnol. Oceanogr.* 48, 843–859
- 457 Behrenfeld, M. J., O'Malley, T., R., Siegel, D. A., R., M. C., Sarmiento, J. L., et al. (2006). Climate-driven
458 trends in contemporary ocean productivity. *Nature* 444, 752–755. doi:doi:10.1038/nature05317
- 459 Bidigare, R. R., Morrow, J. H., and Kiefer, D. A. (1989). Derivative analysis of spectral absorption by
460 photosynthetic pigments in the western sargasso sea. *Journal of Marine Research* 47, 323–341
- 461 Brewin, R. J. W., Hardman-Mountford, N. J., Lavender, S. J., Raitsos, D. E., Hirata, T., Uitz, J., et al. (2011).
462 An intercomparison of bio-optical techniques for detecting phytoplankton size class from satellite remote
463 sensing. *Remote Sensing Env.* 115, 325–339. doi:10.1016/j.rse.2010.09.004
- 464 Bricaud, A., Babin, M., Claustre, H., Rase, J., and Tiéche, F. (2010). Light absorption properties
465 and absorption budget of southeast pacific waters. *Journal of Geophysical Research: Oceans* 115.
466 doi:<https://doi.org/10.1029/2009JC005517>
- 467 Bricaud, A., Babin, M., Morel, A., and Claustre, H. (1995). Variability in the chlorophyll-specific
468 absorption coefficients of natural phtoplankton: Analysis and parameterization. *J. Geophys. Res.* 100,
469 13,321–13,332
- 470 Bricaud, A., Claustre, H., and Oubelkheir, K. (2004). Natural variability of phytoplankton absorption
471 in oceanic waters: influence of the size structure of algal populations. *J. Geophys. Res. Oceans* 110.
472 doi:10.1029/2004JC002419
- 473 Bricaud, A., Mejia, C., Blondeau-Patissier, D., Claustre, H., and and. S. Thiria, M. C. (2007). Retrieval
474 of pigment concentrations and size structure of algal populations from their absorption spectra using
475 multilayered perceptrons. *Appl. Opt.* 46, 1251–1260

- 476 Bricaud, A., Morel, A., Babin, M., Allali, K., and Claustre, H. (1998). Variations of light absorption
477 by suspended particles with chlorophyll a concentration in oceanic waters: Analysis and implications
478 for bio-optical models. *Journal of Geophysical Research: Oceans* 103, 31033–31044. doi:10.1029/
479 98JC02712
- 480 Casault, B., Johnson, C., Devred, E., Head, E. J. H., Cogswell, A., and Spry, J. (2020). Optical, chemical,
481 and biological oceanographic conditions on the scotian shelf and in the eastern gulf of maine during
482 2019. In *Can. Sci. Advis. Sec. Res. Doc.* (DFO). 64
- 483 Catlett, D. and Siegel, D. A. (2018). Phytoplankton pigment communities can be modeled using uni-
484 que relationships with spectral absorption signatures in a dynamic coastal environment. *Journal of*
485 *Geophysical Research: Oceans* 123, 246–264. doi:10.1002/2017JC013195
- 486 Chase, A., Boss, E., Zaneveld, R., Bricaud, A., Claustre, H., Ras, J., et al. (2013). Decomposition of in situ
487 particulate absorption spectra. *Methods in Oceanography* 7, 110–124. doi:<https://doi.org/10.1016/j.mio.2014.02.002>. Special Issue: Advances in Ocean Optical Observing
- 488 Chazottes, A., Bricaud, A., Crépon, M., and Thiria, S. (2006). Statistical analysis of a database of
489 absorption spectra of phytoplankton and pigment concentrations using self-organizing maps. *Appl. Opt.*
490 45, 8102–8115. doi:10.1364/AO.45.008102
- 491 Churilova, T., Suslin, V., Krivenko, O., Efimova, T., Moiseeva, N., Mukhanov, V., et al. (2017). Light
492 absorption by phytoplankton in the upper mixed layer of the black sea: Seasonality and parametrization.
493 *Frontiers in Marine Science* 4. doi:10.3389/fmars.2017.00090
- 494 Ciotti, A. M., Cullen, J. J., and Lewis, M. R. (2002). Assessment of the relationships between domi-
495 nant cell size in natural phytoplankton communities and the spectral shape of absorption coefficient.
496 *Limnol. Oceanogr.* 47, 404–417
- 497 Claustre, H. (1994). The trophic status of various oceanic provinces as revealed by phytoplankton pigment
498 signatures. *Limnol. Oceanogr.* 39, 1206–1210
- 499 Cleveland, J. S. (1995). Regional models for phytoplankton absorption as a function of chlorophyll a
500 concentration. *J. Geophys. Res.* 100, 13,333–13,344
- 501 Collos, Y., Husseini, J. R., Bec, B., Vaquer, A., Lam, H., Rougier, C., et al. (2005). Pheopigment dynamics,
502 zooplankton grazing rates and the autumnal ammonium peak in a mediterranean lagoon. *Hydrobiologia*
503 550, 83–93. doi:10.1007/s10750-005-4365-1
- 504 Devred, E., Sathyendranath, S., Stuart, V., Maass, H., Ulloa, O., and Platt, T. (2006). A two-component
505 model of phytoplankton absorption in the open ocean: theory and applications. *J. Geophys. Res.* 111
- 506 Devred, E., Sathyendranath, S., Stuart, V., and Platt, T. (2011). A three component classification of
507 phytoplankton absorption spectra: Application to ocean-color data. *Remote Sensing Env.* 115, 2255–2266.
508 doi:10.1016/j.rse.2011.04.025
- 509 Dutkiewicz, S., Hickman, A. E., Jahn, O., Henson, S., Beaulieu, C., and Monier, E. (2019). Ocean colour
510 signature of climate change. *Nature Communications* 10, 578. doi:10.1038/s41467-019-08457-x
- 511 Duysens, L. M. N. (1956). The flattening of absorption spectrum of suspensions, as compared to that of
512 solutions. *Biochim. Biophys. Acta* 19, 1–12
- 513 Ferreira, A., Ciotti, A. M., C. R. B. Mendes, C. R. B., Uitz, J., and Bricaud, A. (2017). Phytoplankton
514 light absorption and the package effect in relation to photosynthetic and photoprotective pigments in
515 the northern tip of antarctic peninsula. *Journal of Geophysical Research: Oceans* 122, 7344–7363.
516 doi:<https://doi.org/10.1002/2017JC012964>
- 517 Ferreira, A., Stramski, D., Garcia, C. A. E., Garcia, V. M. T., Ciotti, A. M., and Mendes, C. R. B. (2013).
518 Variability in light absorption and scattering of phytoplankton in patagonian waters: Role of community
519 size structure and pigment composition. *Journal of Geophysical Research: Oceans* 118, 698–714.

- 521 doi:10.1002/jgrc.20082
- 522 Fragoso, G. M., Poulton, A. J., Yashayaev, I., Head, E. J. H., Johnsen, G., and Purdie, D. A. (2018). Diatom
523 biogeography from the labrador sea revealed through a trait-based approach. *Frontiers in Marine Science*
524 5. doi:10.3389/fmars.2018.00297
- 525 Fragoso, G. M., Poulton, A. J., Yashayaev, I., Head, E. J. H., and Purdie, D. A. (2017). Spring phytoplankton
526 communities of the labrador sea (2005–2014): pigment signatures, photophysiology and elemental ratios.
527 *Biogeosciences* 14, 1235–1259. doi:10.5194/bg-14-1235-2017
- 528 Fujiki, T. and Tagushi, S. (2002). Variability in chlorophyll a specific absorption coefficient in marine
529 phytoplankton as a function of cell size and irradiance. *J. Plankton Res.* 24, 859–874
- 530 Gordon, H. R. and McCluney, W. R. (1975). Estimation of the depth of sunlight penetration in the sea for
531 remote sensing. *Appl. Opt.* 14, 413–416
- 532 Head, E. J. H. and Horne, E. P. W. (1993). Pigment transformation and vertical flux in an area of
533 convergence in the north atlantic. *Deep-Sea Res. II* 40, 329–346
- 534 Hieronymi, M., Mueller, D., and Doerffer, R. (2017). The olci neural network swarm (onns): A bio-geo-
535 optical algorithm for open ocean and coastal waters. *Frontiers in Marine Science* 4. doi:10.3389/fmars.
536 2017.00140
- 537 Hirata, T., Aiken, J., Smyth, T. J., Hardman-Mountford, N., and Barlow, R. G. (2008). An absorption model
538 to derive phytoplankton size classes from satellite ocean colour. *Remote Sensing Env.*, 3153–3159
- 539 Hoepffner, N. and Sathyendranath, S. (1991). Effect of pigment composition on absorption properties of
540 phytoplankton. *Mar. Ecol. Prog. Ser.* 73, 11–23
- 541 Hoepffner, N. and Sathyendranath, S. (1993). Determination of the major groups of phytoplankton
542 pigments from the absorption spectra of total particulate matter. *J. Geophys. Res.* 98, 22,789–22,803
- 543 Hoge, F. E. and Lyon, P. E. (1999). Spectral parameters of inherent optical property models: method
544 for satellite retrieval by matrix inversion of an oceanic radiance model. *Appl. Opt.* 38, 1657–1662.
545 doi:10.1364/AO.38.001657
- 546 Kirk, J. T. O. (1976). A theoretical analysis of the contribution of algal cells to the attenuation of light within
547 natural waters. *New Phytologist* 77, 341–358. doi:<https://doi.org/10.1111/j.1469-8137.1976.tb01524.x>
- 548 Kratzer, S. and Moore, G. (2018). Inherent optical properties of the baltic sea in comparison to other seas
549 and oceans. *Remote Sensing* 10. doi:10.3390/rs10030418
- 550 Kyewalyanga, M. N., Platt, T., and Sathyendranath, S. (1997). Estimation of the photosynthetic action
551 spectrum: Implication for primary production models. *Mar. Ecol. Prog. Ser.* 146, 207–223
- 552 Lee, Z. P., Carder, K. L., and Arnone, R. (2002). Deriving inherent optical properties from water color: A
553 multi-band quasi-analytical algorithm for optically deep waters. *Appl. Opt.* 41, 5755–5772
- 554 Leising, A. W., Pierson, J. J., Halsband-Lenk, C., Horner, R., and Postel, J. (2005). Copepod grazing
555 during spring blooms: Does calanus pacificus avoid harmful diatoms? *Progress in Oceanography* 67,
556 384–405. doi:10.1016/j.pocean.2005.09.008. Diatom Blooms and Copepod Responses: Paradigm or
557 Paradox?
- 558 Liu, X., Devred, E., and Johnson, C. (2018). Remote sensing of phytoplankton size class in northwest
559 atlantic from 1998 to 2016: Bio-optical algorithms comparison and application. *Remote. Sens.* 10, 1028.
560 doi:10.3390/rs10071028
- 561 Maritorena, S., Siegel, D. A., and Peterson, A. R. (2002). Optimization of a semi-analytical ocean color
562 model for global-scale applications. *Appl. Opt.* 41, 2705–2713
- 563 Marra, J., Trees, C. C., and O'Reilly, J. E. (2007). Phytoplankton pigment absorption: A strong predictor of
564 primary productivity in the surface ocean. *Deep Sea Research Part I: Oceanographic Research Papers*
565 54, 155–163. doi:<https://doi.org/10.1016/j.dsr.2006.12.001>

- 566 Mascarenhas, V. J., Voss, D., Wollschlaeger, J., and Zielinski, O. (2017). Fjord light regime: Bio-optical
567 variability, absorption budget, and hyperspectral light availability in sognefjord and trondheimsfjord,
568 norway. *Journal of Geophysical Research: Oceans* 122, 3828–3847. doi:<https://doi.org/10.1002/2016JC012610>
- 570 Matsuoka, A., Babin, M., Doxaran, D., Hooker, S. B., Mitchell, B. G., Bélanger, S., et al. (2014). A
571 synthesis of light absorption properties of the arctic ocean: application to semianalytical estimates of
572 dissolved organic carbon concentrations from space. *Biogeosciences* 11, 3131–3147. doi:10.5194/bg-11-3131-2014
- 574 Mitchell, B. G. and Kiefer, B. A. (1984). Determination of absorption and fluorescence excitation spectra
575 for phytoplankton. In *Marine phytoplankton and productivity*, eds. O. Holm-Hansen, L. Bolis, and
576 R. Giles (Berlin Heidelberg: Springer-Verlag). 157–169
- 577 Mitchell, B. G. and Kiefer, B. A. (1988). Variability in pigment specific particulate fluorescence and
578 absorption spectra in the northeast Pacific Ocean. *Deep-Sea Res.* 28, 1375–1393
- 579 Mobley, C. D. (1994). Optical properties of water. In *Light and Water: Radiative Transfer in Natural
580 Waters*, eds. O. Holm-Hansen, L. Bolis, and R. Giles (London: Academic Press). 61–142
- 581 Moran, M. A. and Zepp, R. G. (1997). Role of photoreactions in the formation of biologically labile
582 compounds from dissolved organic matter. *Limnology and Oceanography* 42, 1307–1316. doi:<https://doi.org/10.4319/lo.1997.42.6.1307>
- 584 Morel, A. (1978). Available, usable, and stored radiant energy in relation to marine photosynthesis. *Deep
585 Sea Research* 25, 673–688. doi:[https://doi.org/10.1016/0146-6291\(78\)90623-9](https://doi.org/10.1016/0146-6291(78)90623-9)
- 586 Morel, A. and Bricaud, A. (1981). Theoretical results concerning light absorption in a discrete medium,
587 and application to specific absorption of phytoplankton. *Deep Sea Res.* 28, 1375–1393
- 588 Morel, A. and Prieur, L. (1977). Analysis of variation in ocean color. *Limnol. Oceanogr.* 22, 709–722
- 589 Nagasaki, K. (2008). Dinoflagellates, diatoms, and their viruses. *Journal of microbiology (Seoul, Korea)*
590 46, 235–43. doi:10.1007/s12275-008-0098-y
- 591 Oubelkheir, K., Claustre, H., Bricaud, A., and Babin, M. (2007). Partitioning total spectral absorption in
592 phytoplankton and colored detrital material contributions. *Limnology and Oceanography: Methods* 5,
593 384–395. doi:<https://doi.org/10.4319/lom.2007.5.384>
- 594 Pepin, P., Petrie, B., Therriault, J.-C., Narayanan, S., Harrisson, W., Frank, K., et al. (2005). The atlantic
595 zone monitoring program (azmp): Review of 1998-2003. *Can. Tech. Rep. Hydrogr. Ocean Sci.* 242, 57
- 596 Platt, T. and Gallegos, C. L. (1980). *Modelling Primary Production* (Boston, MA: Springer US). 339–362.
597 doi:10.1007/978-1-4684-3890-1_19
- 598 Pérez, G. L., Galí, M., Royer, S.-J., Gerea, M., Ortega-Retuerta, E., Gasol, J. M., et al. (2021). Variability
599 of phytoplankton light absorption in stratified waters of the nw mediterranean sea: The interplay between
600 pigment composition and the packaging effect. *Deep Sea Research Part I: Oceanographic Research
601 Papers* 169, 103460. doi:<https://doi.org/10.1016/j.dsr.2020.103460>
- 602 Sathyendranath, S., Watts, L., Devred, E., Platt, T., Caverhill, C., and Maass, H. (2004). Discrimination of
603 diatoms from other phytoplankton using ocean-colour data. *Mar. Ecol. Prog. Ser.* 272, 59–68
- 604 Shuman, F. R. and Lorenzen, C. J. (1975). Quantitative degradation of chlorophyll by a marine herbivore.
605 *Limnology and Oceanography* 20, 580–586. doi:<https://doi.org/10.4319/lo.1975.20.4.0580>
- 606 Sosik, H. M. and Mitchell, B. G. (1992). A comparison of particulate absorption properties between high-
607 and mid-latitude surface waters. *Antarctic. J. United States* 27, 162–164
- 608 Staehr, A., Markager, S., and Sand-Jensen, K. (2004). Pigment specific in vivo light absorption of
609 phytoplankton from estuarine, coastal and oceanic waters. *Marine Ecology Progress Series* 275,
610 115–128. doi:10.3354/meps275115

- 611 Stramski, D., Reynolds, R. A., Kaczmarek, S., Uitz, J., and Zheng, G. (2015). Correction of pathlength
612 amplification in the filter-pad technique for measurements of particulate absorption coefficient in the
613 visible spectral region. *Appl. Opt.* 54, 6763–6782. doi:10.1364/AO.54.006763
- 614 Stuart, V., Sathyendranath, S., Head, E. J. H., Platt, T., Irwin, B. D., and Maas, H. (2000). Bio-optical
615 characteristics of diatom and prymnesiophyte populations in the Labrador Sea. *Mar. Ecol. Prog. Ser.*
616 201, 91–106
- 617 Teegarden, G. J., Campbell, R. G., and Durbin, E. G. (2001). Zooplankton feeding behavior and particle
618 selection in natural plankton assemblages containing toxic *Alexandrium* spp. *Marine Ecology Progress Series*
619 218, 213–226. doi:10.3354/meps218213
- 620 Therriault, J.-C., Petrie, B., P. Pépin, J. G., Gregory, D., Helbig, J., Herman, A., et al. (1998). Proposal for
621 a northwest atlantic zonal monitoring program. In *Can. Tech. Rep. Hydrogr. Ocean Sci.* (DFO), vol. 194.
622 vii+57
- 623 Trees, C. C., Clark, D. K., Bidigare, R. R., Ondrusek, M. E., and Mueller, J. L. (2000). Accessory
624 pigments versus chlorophyll *a* concentrations within the euphotic zone: An ubiquitous relationship.
625 *Limnol. Oceanogr.* 45, 1130–1143
- 626 Uitz, J., Claustre, H., Morel, A., and Hooker, S. B. (2006). Vertical distribution of phytoplankton
627 communities in open ocean: An assessment based on surface chlorophyll. *J. Geophys. Res.* 111.
628 doi:10.1029/2005jc003207
- 629 Vandermeulen, R. A., Mannino, A., Craig, S. E., and Werdell, P. J. (2020). 150 shades of green: Using the
630 full spectrum of remote sensing reflectance to elucidate color shifts in the ocean. *Remote Sensing of*
631 *Environment* 247, 111900. doi:<https://doi.org/10.1016/j.rse.2020.111900>
- 632 Vidussi, F., Claustre, H., Manca, B. B., Luchetta, A., and Marty, J. C. (2001). Phytoplankton pigment
633 distribution in relation to upper thermocline circulation in the eastern Mediterranean Sea during winter.
634 *J. Geophys. Res.* 106, 19,939–19,956
- 635 Vishnu, P., Shaju, S., Tiwari, S., Menon, N., Nashad, M., Joseph, C. A., et al. (2018). Seasonal variability
636 in bio-optical properties along the coastal waters off cochin. *International Journal of Applied Earth*
637 *Observation and Geoinformation* 66, 184–195. doi:10.1016/j.jag.2017.12.002
- 638 Werdell, J., Mckinna, L., Boss, E., Ackleson, S., Craig, S., W. Gregg, W., et al. (2018). An overview of
639 approaches and challenges for retrieving marine inherent optical properties from ocean color remote
640 sensing. *Progress in Oceanography* 160. doi:10.1016/j.pocean.2018.01.001
- 641 Williams, G. N., Larouche, P., Dogliotti, A. I., and Latorre, M. P. (2018). Light absorption by phytoplankton,
642 non-algal particles, and dissolved organic matter in san jorge gulf in summer. *Oceanography* 31, 40–49.
643 doi:10.5670/oceanog.2018.409
- 644 Yashayaev, I., Peterson, I., and Wang, Z. (2021). Meteorological, sea ice, and physical oceanographic
645 conditions in the labrador sea during 2018. In *Can. Sci. Advis. Sec. Res. Doc.* (DFO), vol. 42. 26
- 646 Zhang, Y., Wang, G., Sathyendranath, S., Xu, W., Xiao, Y., and Jiang, L. (2021). Retrieval of phytoplankton
647 pigment composition from their in vivo absorption spectra. *Remote Sensing* 13. doi:10.3390/rs13245112

TABLES

- 648 The N here does really make sense, as for example, the number of chla and snap are likely not the same for
649 a given season/region.

Season	<i>N</i>	[Chl-a]	[Fuco]	$a_\phi(443)$	$a_\phi^*(443)$	$a_{NAP}(443)$	S_{NAP}	$PAAW$
All data	2267							
Scotian Shelf								
Spring	781	2.70 (0.102-13.6)	0.89 (0.000-6.68)	0.049 (0.004-0.216)	0.0297 (0.004-0.1636)	0.009 (0.0002-0.0378)	0.0124 (0.0018-0.0275)	
Summer	36	0.32 (0.093-0.882)	0.03 (0.000-0.131)	0.022 (0.009-0.057)	0.0781 (0.0321-0.133)	0.0042 (0.001-0.0132)	0.0118 (0.0062-0.0195)	
Autumn	781	0.83 (0.080-4.13)	0.13 (0.000-1.68)	0.050 (0.007-0.177)	0.0724 (0.0048-0.2896)	0.0065 (0.0004-0.0314)	0.01 (0.0004-0.02)	
Winter	74	0.68 (0.211-1.59)	0.16 (0.053-0.517)	0.032 (0.009-0.064)	0.0493 (0.0212-0.1463)	0.0078 (0.0007-0.0178)	0.0088 (0.006-0.0167)	
Northwest Atlantic Basin								
Spring	313	1.80 (0.091-10.4)	0.47 (0.000-5.37)	0.051 (0.008-0.176)	0.0421 (0.0063-0.1724)	0.0051 (0.0005-0.0419)	0.0131 (0.0001-0.0403)	
Summer	58	0.21 (0.090-0.553)	0.03 (0.000-0.168)	0.017 (0.007-0.037)	0.0890 (0.0598-0.1373)	0.0033 (0.0009-0.0095)	0.0129 (0.005-0.0175)	
Autumn	369	0.400 (0.060-2.19)	0.040 (0.000-0.892)	0.028 (0.009-0.081)	0.0838 (0.0246-0.2305)	0.0036 (0.0002-0.0184)	0.011 (0.003-0.0284)	
Winter	45	0.87 (0.531-2.03)	0.16 (0.031-0.796)	0.032 (0.016-0.054)	0.0389 (0.0204-0.0607)	0.0037 (0.0006-0.0082)	0.0111 (0.0069-0.0186)	
Labrador Sea								
Spring	504	2.73 (0.076-17.5)	0.72 (0.000-4.73)	0.063 (0.004-0.224)	0.0363 (0.0069-0.1428)	0.0075 (0.0004-0.1384)	0.0134 (0.0026-0.0415)	
Summer	275	1.99 (0.10-8.48)	0.67 (0.000-4.43)	0.061 (0.012-0.231)	0.0489 (0.0081-0.2402)	0.0068 (0.0011-0.0289)	0.0106 (0.0012-0.0297)	
Autumn	24	0.88 (0.225-3.19)	0.26 (0.000-1.41)	0.038 (0.014-0.093)	0.0538 (0.0188-0.1069)	0.0031 (0.0004-0.0065)	0.0163 (0.01-0.0228)	
Winter	19	0.19 (0.093-0.321)	0.05 (0.017-0.155)	0.009 (0.004-0.014)	0.0471 (0.0377-0.0521)	0.0017 (0.001-0.0037)	0.0121 (0.0109-0.0139)	

Table 1.

Dataset	slope	p-value	R^2
All	0.083	NS	0.11
Regions			
Scotian Shelf	0.107	NS	0.05
NAB	0.136	NS	0.10
Labrador Sea	0.082	NS	0.08
Regions in Spring			
Scotian Shelf	0.382	< 0.05	0.28
NAB	0.229	< 0.05	0.36
Labrador Sea	0.347	< 0.05	0.32
Regions in Autumn			
Scotian Shelf	-0.155	< 0.05	0.27
NAB	-0.348	< 0.05	0.61

Table 2.

651 What is this table? Looking at it I do not understand what are the slope and the pvalue for. Regressions?
 652 Between what?

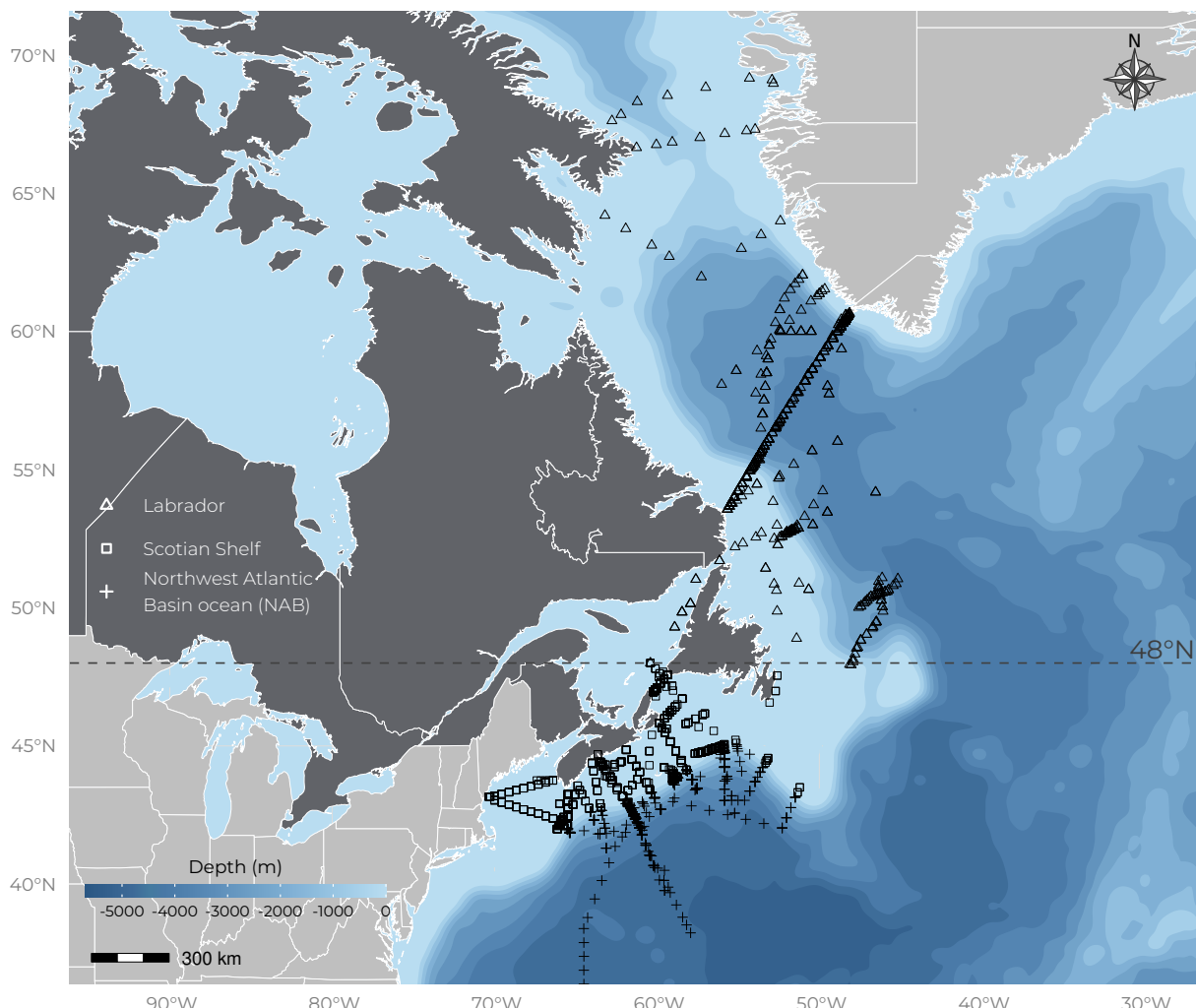
FIGURE CAPTIONS

Figure 1. Location of Samplings. The blue background indicate the bathymetry (see colorbar in bottom left panel). Dark grey corresponds to Canada and light Grey corresponds to other countries (i.e., United States of America and Denmark)

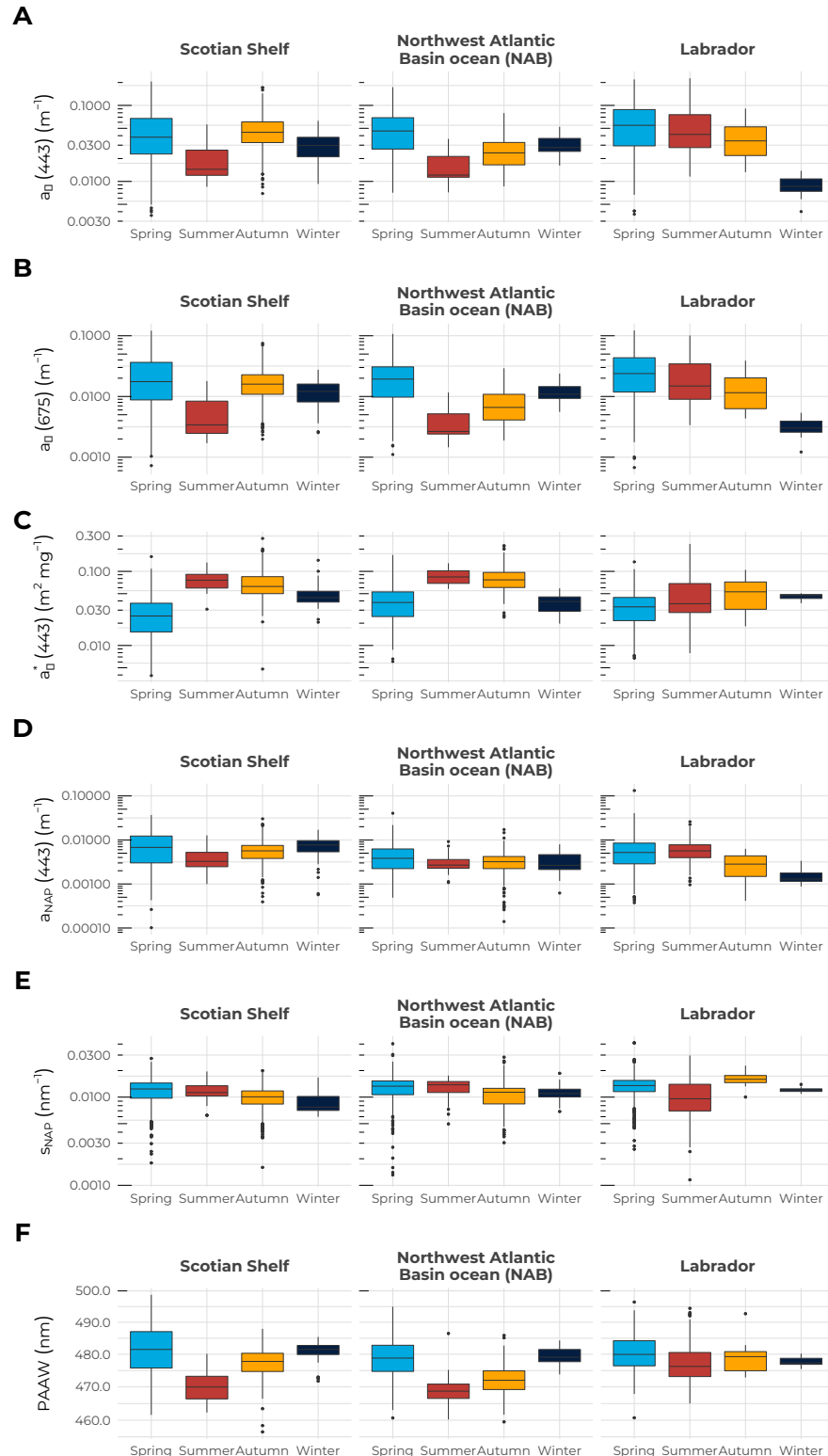


Figure 2. Mean and one standard deviation (i.e., boxplot) of A) $a_\phi(443)$, B) $a_\phi(675)$, C) $a^*(443)$, D) $a_{NAP}(443)$, E) S_{NAP} and F) PAAW for the Scotian Shelf (left column), Northwest Atlantic Ocean (middle column) and Labrador Sea (right column). In each panel, the blue, red, yellow and black boxes correspond to the spring, summer, autumn and winter respectively.

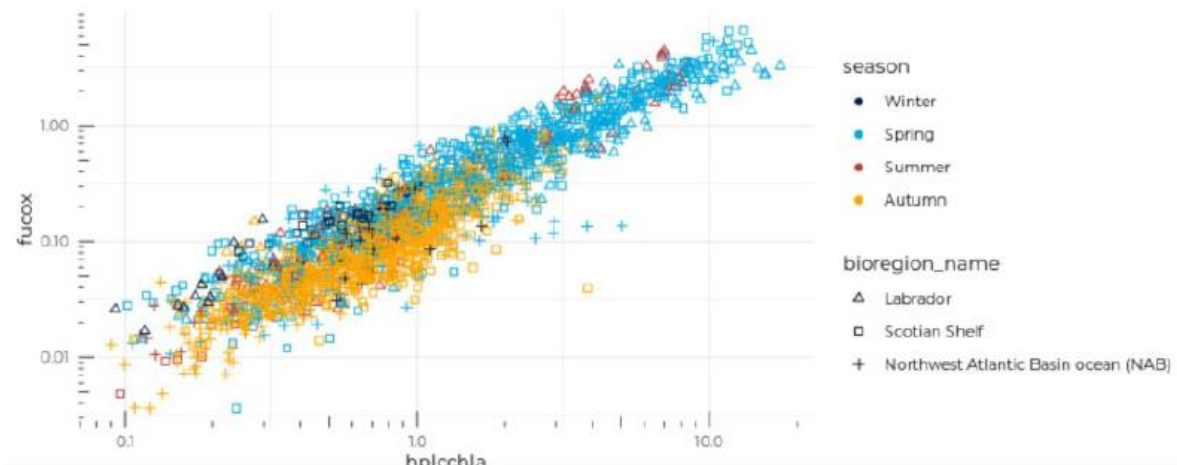


Figure 3. [Fucox] as a function of [Chl-a]. Symbols are colour coded according to season as in Figure 2

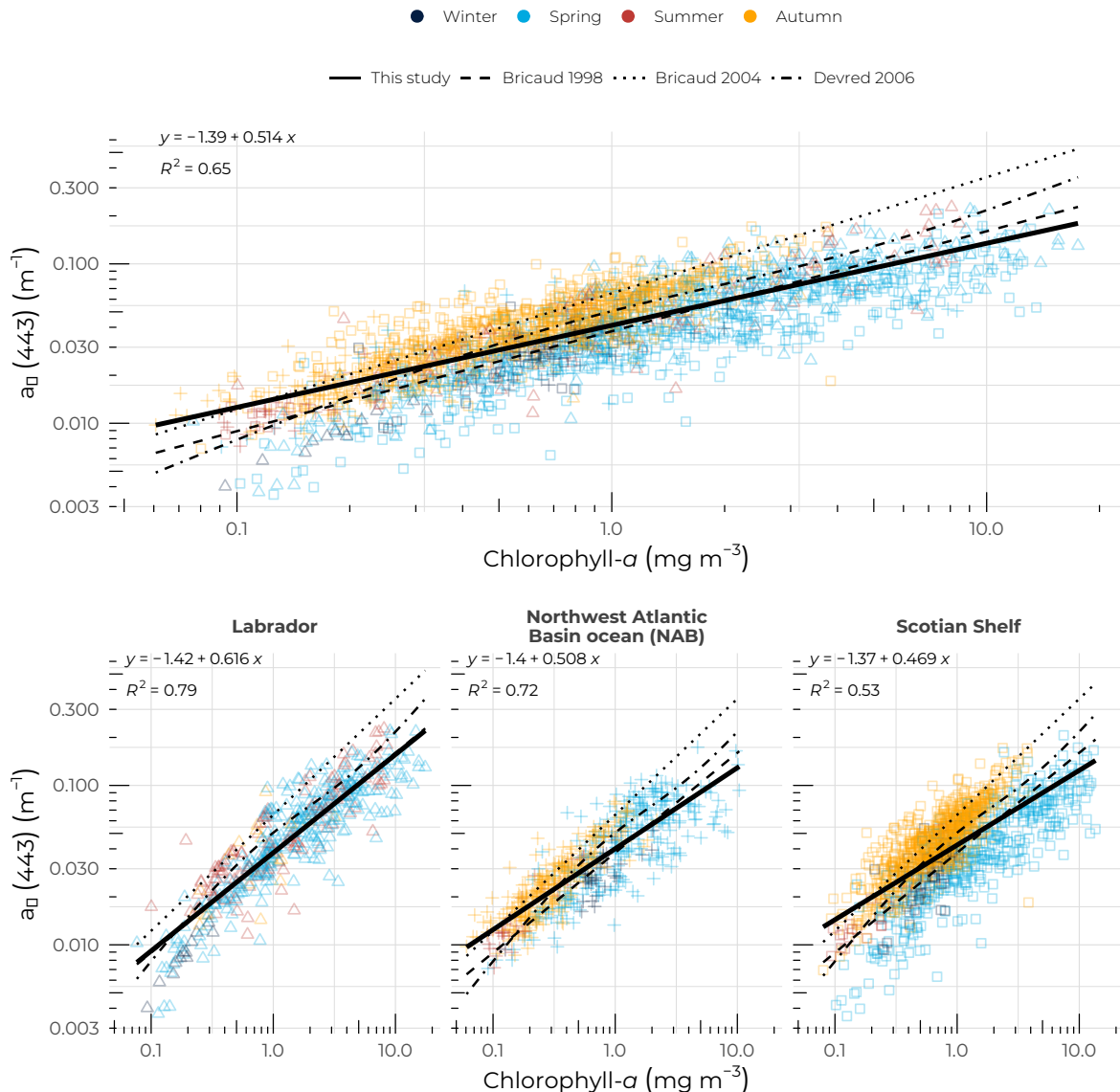


Figure 4. Phytoplankton absorption coefficient at 443 nm, $a_\phi(443)$, as a function of [Chl-a] for A) the entire dataset, B) the Scotian Shelf, C) the Northwest Atlantic Basin and D) the Labrador Sea. The solid black lines correspond to the power law fit (Equation 3.2), the long-dashed, short-dashed and dotted-dashed lines correspond to Bricaud et al. (1998), Bricaud et al. (2004) and Devred et al. (2006) models respectively. Symbols are colour coded according to season as in Figure 2

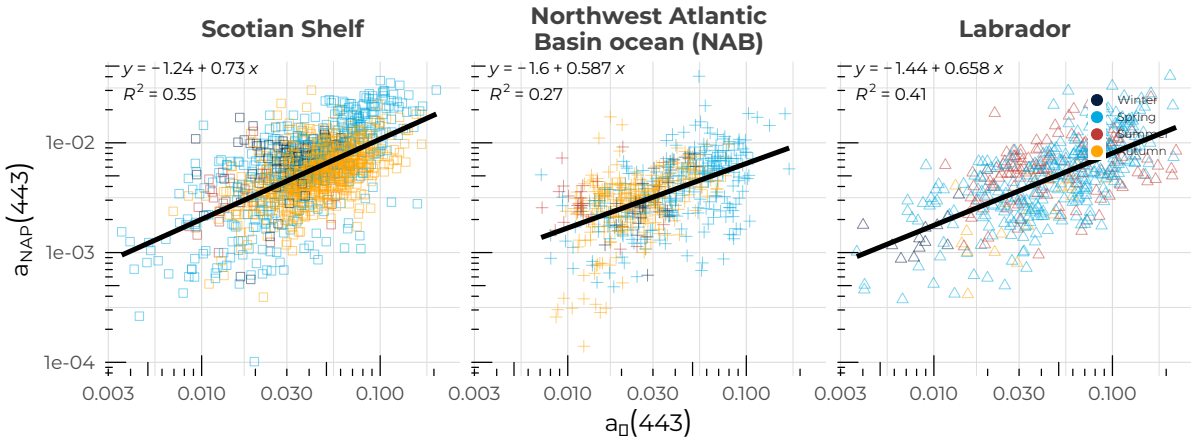


Figure 5. can you group figure 5 and 5b together as in figure 4. I dont know what you mean. In the legend you talk about chl and this figure do not show cha. Also, I do not know what is fig 5b, you changed the figure order. Non-algal particulate absorption coefficient at 443 nm, $a_{NAP}(443)$, as a function of [Chl-a] for A) the entire dataset, B) the Scotian Shelf, C) the Northwest Atlantic Basin and D) the Labrador Sea. The solid black lines correspond to the power law fit (Equation 3.2), the long-dashed, short-dashed and dotted-dashed lines correspond to Bricaud et al. (1998), Bricaud et al. (2004) and Devred et al. (2006) models respectively. Symbols are colour coded according to season as in Figure 2

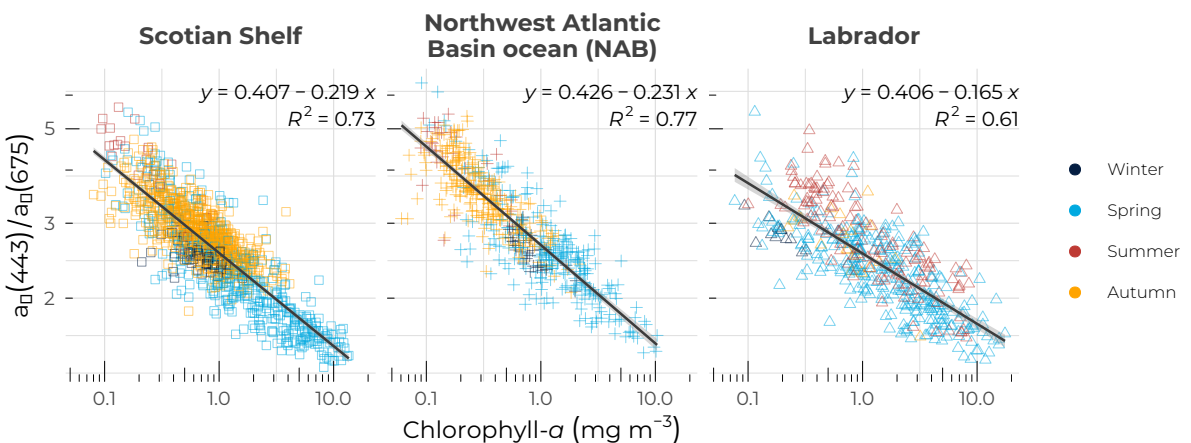


Figure 6. Ratio of $a_\phi(443)$ to $a_\phi(675)$ as a function of [Chl-a] for the Scotian Shelf (left), Northwest Atlantic Basin (middle) and Labrador Sea (right). Symbols are colour coded according to season as in Figure 2

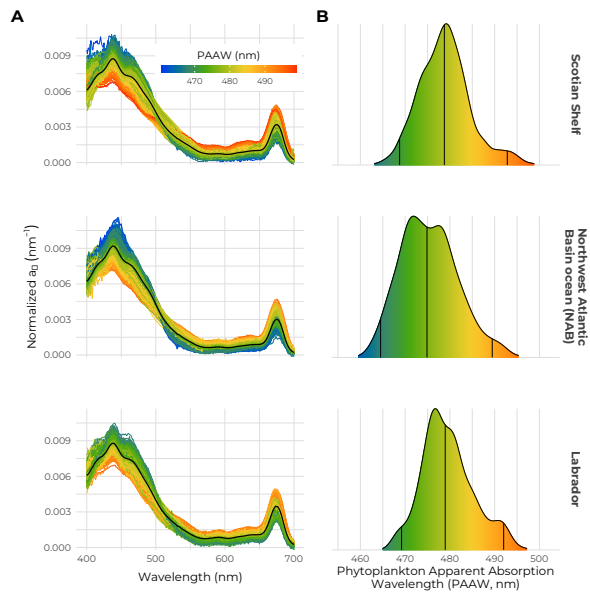


Figure 7. A) Phytoplankton absorption spectra and B) distribution of the *PAAW* for the Scotian Shelf (top), NAB (middle) and Labrador Sea (bottom), the color bar indicate the *PAAW* values in all panels.

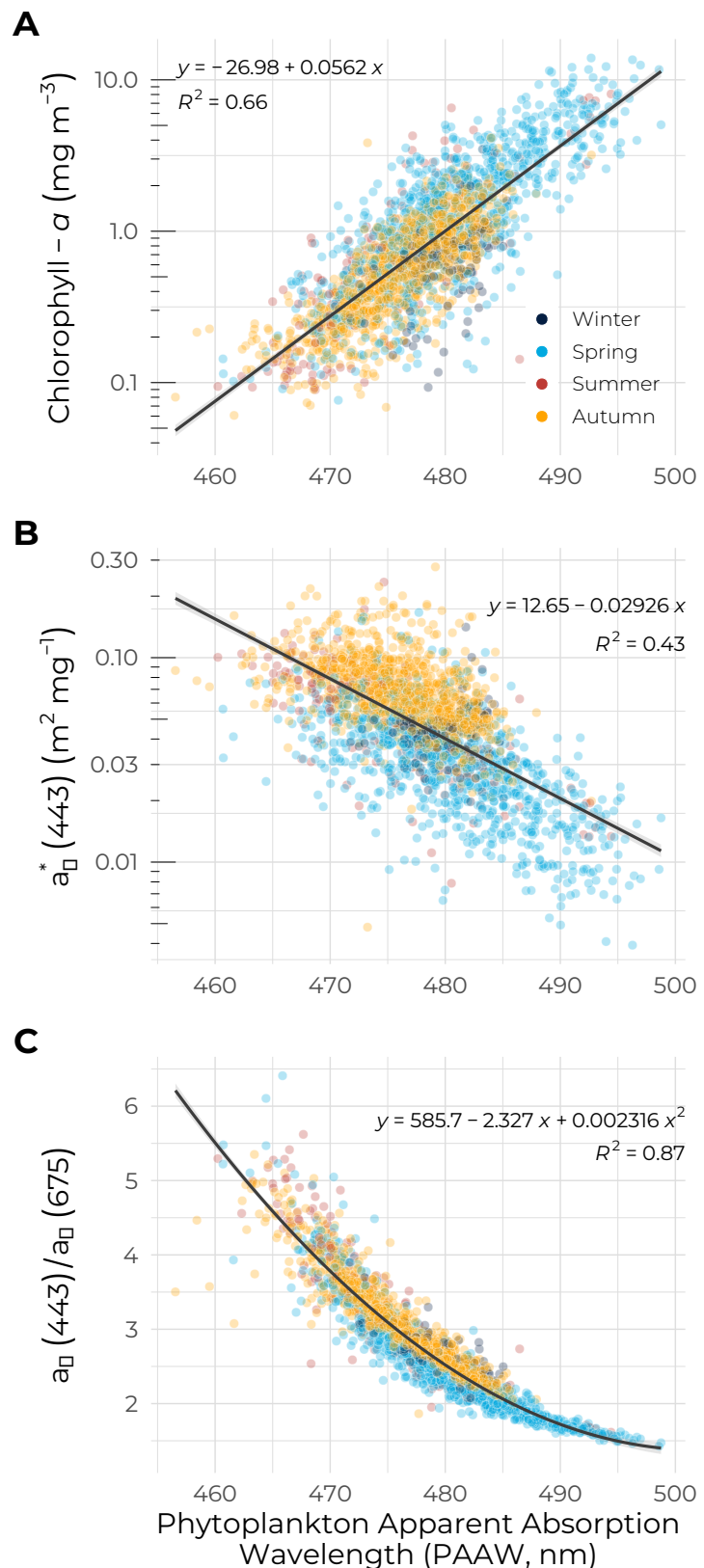


Figure 8. A) [Chl-a], B) $a_\phi^{*}(443)$ and C) $a_\phi(443) : a_\phi(675)$ as a function of PAAW for the entire dataset

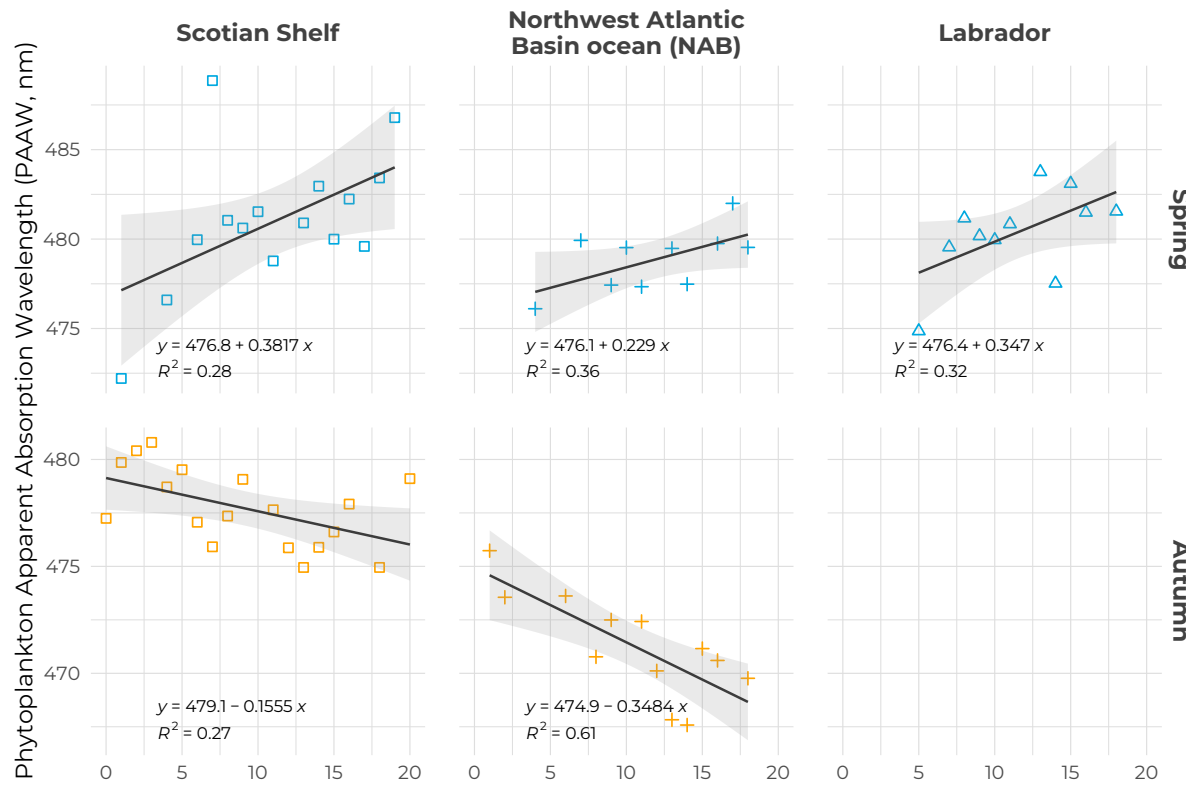


Figure 9. Seasonal trends in *PAAW* for spring (top panels) and autumn (bottom panels) for the Scotian Shelf (left), NAB (middle) and Labrador Sea (right). The black solid lines correspond to the linear regression of *PAAW* against time with the coefficient and R^2 indicated in each panel. Symbols are colour coded according to season as in Figure 2

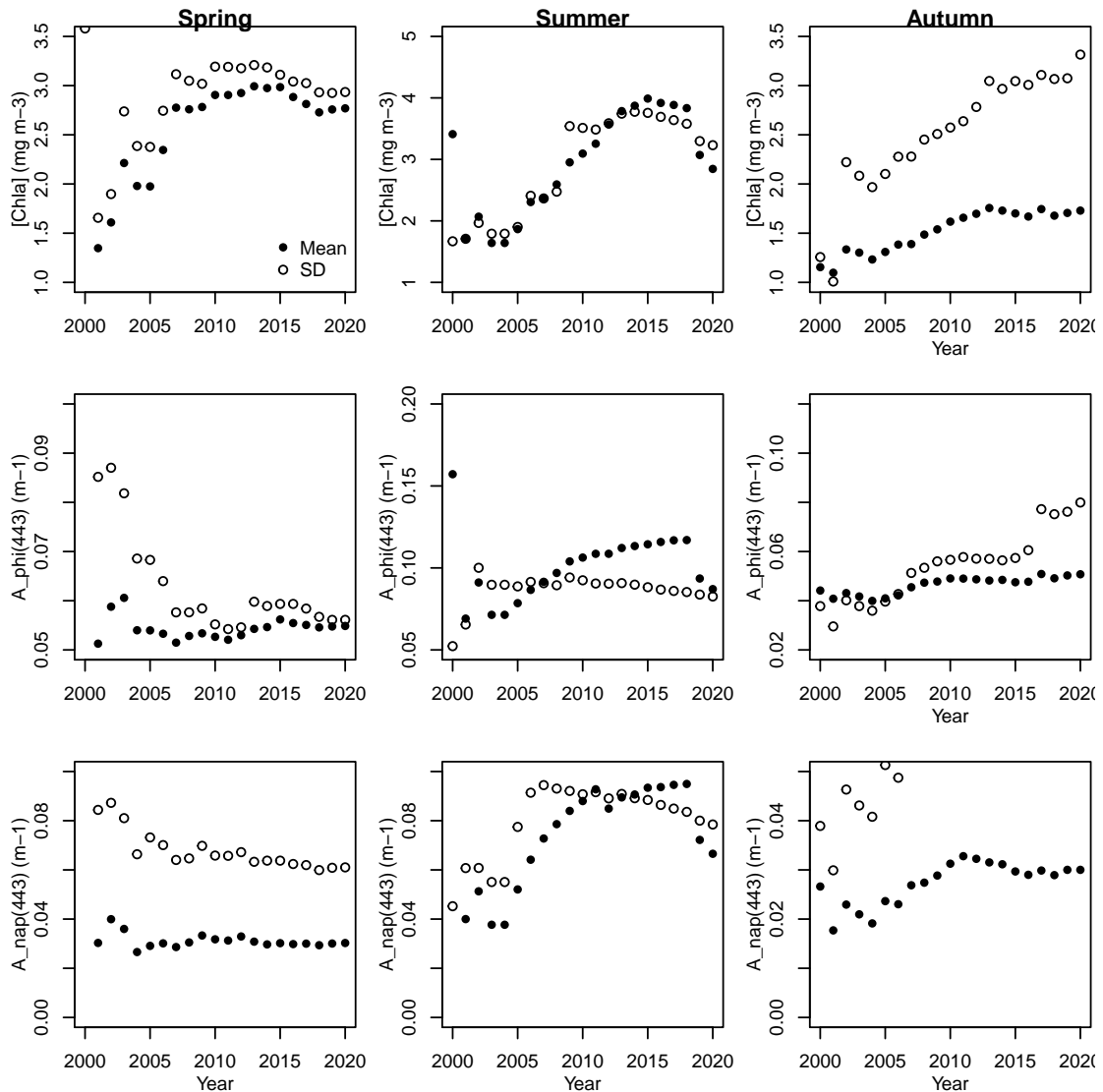


Figure 10. Mean (solid black circles) and standard deviation (open black circle) as a function of time for [Chl-a] (top), $a_{\phi}(443)$ (middle) and $a_{NAP}(443)$ (bottom) (you should use text mode to write NAP instead of math mode, it does not look good) in spring (left column), summer (middle column) and autumn (right column on the Scotian Shelf